applied sciences

MDPI

Article

Numerical Analysis of the Effects of the Structure Shape and Orientation of Kelvin Cell Porous Structures during Air Forced Convection

Michele Calati, Edoardo De Monte and Simone Mancin *

Department of Management and Engineering, University of Padova, Str.lla S. Nicola, 3, 36100 Vicenza, Italy; michele.calati@phd.unipd.it (M.C.); edoardo.demonte@studenti.unipd.it (E.D.M.)
* Correspondence: simone.mancin@unipd.it

Abstract: In recent years, in order to counteract the growth of environmental pollution and the contemporary scarcity of various energy sources, researchers have proposed innovative and efficient solutions for heat transfer applications. Extended surfaces, which can involve the use of fins, open cell metal foams, etc., have been demonstrated to be promising solutions. Open cell metal foams consist of structs intersecting at nodes resulting in stochastic oriented cells. Periodic metal foams have also attracted great interest. These structures are made of a single cell unit periodically replicated. Kelvin cells and Weaire–Phelan ones are two conventional elementary unit cells. In this paper, a numerical model is developed and validated, aiming at analysing the thermal and hydraulic behaviors of modified Kelvin cell-based metal foams during air forced convection. Constant porosity (0.9) and pore density (40 PPI) were adopted. Five different geometrical configurations (one cylindrical and four elliptical) and four orientations (0–15–30–45°) of the struts with respect to the main air flow direction were investigated. The inlet air velocities varied between 0.5 and 4 m s^{-1}. Interesting results were obtained and discussed in terms of pressure drops, heat transfer coefficients, and pumping power per area density.

Keywords: air forced convection; Kelvin cells; metal foams; pressure drops; heat transfer enhancement

Citation: Calati, M.; De Monte, E.; Mancin, S. Numerical Analysis of the Effects of the Structure Shape and Orientation of Kelvin Cell Porous Structures during Air Forced Convection. *Appl. Sci.* **2021**, *11*, 6189. https://doi.org/10.3390/app11136189

Academic Editor: Michele Celli

Received: 3 June 2021
Accepted: 1 July 2021
Published: 3 July 2021

1. Introduction

In the last years, open cell metal foams have been extensively investigated [1]. Metal foams are cellular structured materials consisting of stochastically oriented open cells. Their struts interconnect at nodes assuming the conventional shape of an open cell. Stochastic metal foams have specific features which make them suitable to be implemented and integrated in different applications related to heat transfer processes [2]. Open foams are characterized by high heat transfer area to volume ratio, attractive stiffness and strength, and they possess the ability to enhance the flow mixing. As an enhancement heat transfer technique, metal foams can be adopted in different fields, for instance: biomedical, geothermal operations, multifunctional heat exchangers, and cladding on buildings, as an air cooling means for condensers or for acting as compact heat sinks for power electronics. They have been proposed to be an interesting solution to solve the limited air cooling capacity in electronic equipment [3]. The thermal-hydraulic behavior of stochastic metal foams depends upon their geometrical characteristics such as the pore diameter, the pore density (number of pores per linear inch), struts diameter and length, the porosity, and the relative density as well as on the operating conditions. The porosity and the relative density are defined as the ratio between the volume of void and the total volume, and the ratio between density of the foam and of the metal one, respectively [2].

Extensive experimental studies involving open cell foams can be retrieved in the open literature. The influence of geometrical features on the pressure drop and heat transfer

performance were investigated by Lu et al. [4]. Adopting the Brinkman-extended Darcy momentum model and a heat transfer one developed for porous structures based on two equations, they obtained that, compared with the reference tubes, the metal foams performed up to 40 times better if considering the heat transfer. Aluminum metal foams with pore densities ranging from 10 to 45 PPI and porosities from 75% to 85% were used by Incera Garrido et al. [5]. The authors aimed at analysing mass transfer and pressure drop properties. Results revealed that the higher the pore density, the higher the pressure drops. On the contrary, the lower the porosity, the higher the pressure drops. Yu et al. [6] investigated the air forced convection using five graphite foams. By means of an electrical device, the samples were heated and thermal properties were analyzed. The authors stated that the pressure drop increases as the pore dimension decreases whilst the thermal performance improves as the inlet velocity increases. Kim et al. [7] focused on forced convection across aluminum foams to study the effect of the porosity on the heat transfer performance. Three samples had constant porosity (0.92) and pore densities between 10 and 40 PPI, while the other three presented different porosities but constant pore density (20 PPI). Zhao et al. [8] experimentally evaluated the thermal-hydraulic behavior of six copper alloy foams. They measured heat transfer coefficient and pressure drops, finding that the overall heat transfer was affected by cell size more than by porosity. Aiming at obtaining a trade-off between pressure drops and heat transfer, Zhao et al. [8] proposed an optimal porosity which rose as Reynolds number reduced. Abadi et al. [9] experimentally investigated 20 to 60 PPI metal foams by measuring heat transfer coefficient and pressure drop. If compared to the compact-plate heat exchanger with empty channels, the foamed one presented heat transfer coefficients which increased from 3.5 to 5.1 times and pressure drops from 3.2 to 5.7 times.

From this brief overview, stochastic open cell foams can potentially improve the thermal performance in air forced convection as compared to other extended surfaces. At the same time, it was demonstrated how their geometrical parameters highly influenced their performance. Besides, it must be considered that, due to their intrinsic stochastic nature, they cannot be reproduced with always the same geometrical characteristics. It is evident that this can limit their heat transfer enhancement capacity, and, consequently, their adoption in practical applications.

Therefore, periodic metal foams (i.e., known as periodic cellular structures) have recently received great attention by researchers. The potentiality of periodic foams is, undoubtedly, their tunability [10], which can lead to a high level of final product customization [11]. Nowadays, different technologies can support the ordered foam development and diffusion [12]. One of them is the additive manufacturing (AM) technology. The latter has been continuously developing and it is considered suitable to generate complex periodic structures [13] with, in some cases, affordable costs [14].

Pioneering work on ordered foams can be attributed to Lord Kelvin [15]. The author revealed that the best approximation of an open cell foam can be obtained by the replication of a single cell shaped as a tetrakaidecahedron with slightly curved faces. Lord Kelvin [15] considered the so-built tetrakaidecahedron to be the cell shape which caused the surface area per unit volume to be minimized. Starting from Lord Kelvin's [15] work, Weaire and Phelan [16] developed a new structure consisting of 8 isovolumetric polyhedra. Six of them have 14-faced cells (12 pentagonal faces and 2 hexagonal ones) whilst the others are two pentagonal dodecahedra. Compared with a same-volume porous structure made of Lord Kelvin cells, the Weaire and Phelan [16] one leads to a surface area which is some of 0.3% smaller. Even though other models can be retrieved in literature [17–21], Lord Kelvin [15] and Weaire and Phelan [16] ones are considered the best representation of real open cell foams [22].

From a numerical point of view, one approach to investigate thermal-hydraulic behavior of stochastic foams is to firstly reproduce them via tomography-based techniques [23,24] and, successively, importing the obtained foams in a CFD software. It is known that numerical analyses can usually be cheaper than experimental ones. Nevertheless, the generation

of the geometry by means of computational techniques is the cheapest way to describe transport phenomena [22]. Therefore, generating periodic cell foams seems suitable to address this purpose. Iasiello et al. [25] made a comparison between numerically estimated heat transfer coefficients and pressure drops in a structure obtained by means of tomography-based procedure with the same variables calculated in Lord Kelvin's structure. Cunsolo et al. [22] adopted the Lord Kelvin and Weaire–Phelan models to find a simple geometric approximation of an open cell to describe convective heat transfer and pressure drop. The authors compared the two models. Different porosities (0.85, 0.9, 0.95) were tested. In terms of friction factor, Lord Kelvin structures led to 10% always lower values than Weaire–Phelan ones. Therefore, it was stated that the simplest Lord Kelvin cells did not affect the solution accuracy significantly.

As it was affirmed for stochastic open cell foams, geometrical parameters influence the thermo fluid dynamic performance even of the structured porous media. Additionally, in periodic foams, the strut shapes were found to have a not-negligible impact on the thermal-hydraulic behavior. Ambrosio et al. [26] investigated metal foams with concave or convex triangular struts at constant porosity. The authors revealed that the concave one showed better convective heat transfer performance with contemporary lower pressure drop than the convex one. Moon et al. [27] studied pressure drop and heat transfer performance of Kelvin cell-based foams with circular and elliptical struts. In particular, the authors transformed the circular struts into elliptical ones by adopting two different criteria: the first was to maintain the same section strut perimeter while the second was to maintain constant the section area. Different air velocities were tested. The elliptical struts obtained through the first criterion led to 32% lower pumping power being needed if compared with circular struts.

Nevertheless, to the best of the authors' knowledge, the effect of fiber orientation has not been investigated yet. Therefore, in this work, starting from Kelvin cell-based foams developed by Moon et al. [27], four different fiber orientation angles were tested (0, 15, 30, 45°) with respect to the main air flow. Air forced convection was solved by means of numerical simulations run through Ansys Fluent 18.2. Five different air inlet velocities, corresponding to five different Reynolds numbers, were set. Results revealed that by increasing the elliptical struts orientation (up to 30°), a significant reduction in pressure drops as velocity increased, if compared with the circular struts. On the contrary, only the 45° foams presented a worse hydraulic behavior. Focusing on the thermal performance, uniform results were not obtained, and these are accurately discussed in the following sections.

2. Materials and Methods

2.1. Numerical Model—Geometry and Boundary Conditions

The geometrical model was developed based on the work of Moon et al. [27]. Kelvin cell-based metal foams were obtained, arranging in series four single units (Figure 1ii), as shown in Figure 1iii.

Firstly, as reported in Figure 1i, the elementary unit was generated and then replicated by symmetry along its faces resulting in a single Kelvin cell unit (Figure 1ii). As done by Moon et al. [27], five different fiber structures were modeled: one cylindrical (C_0) and four elliptical (E1-1, E1-2, E2-1, E2-2). The configurations denoted as "E1-X" consist of elliptical struts whose section presents the same perimeter with respect to the circular one of the cylindrical fibers. Differently, the "E2-X" were obtained, imposing that the circle and ellipse had equivalent areas. X could assume values of 1 or 2: 1 if the ratio β between the minor strut diameter and the cylindrical strut diameter was 0.815; 2 if the ratio was 0.556. If calculating the ratio α between the major strut diameter and the cylindrical strut diameter, different values for "E1-X" and "E2-X" were obtained, as shown in Table 1.

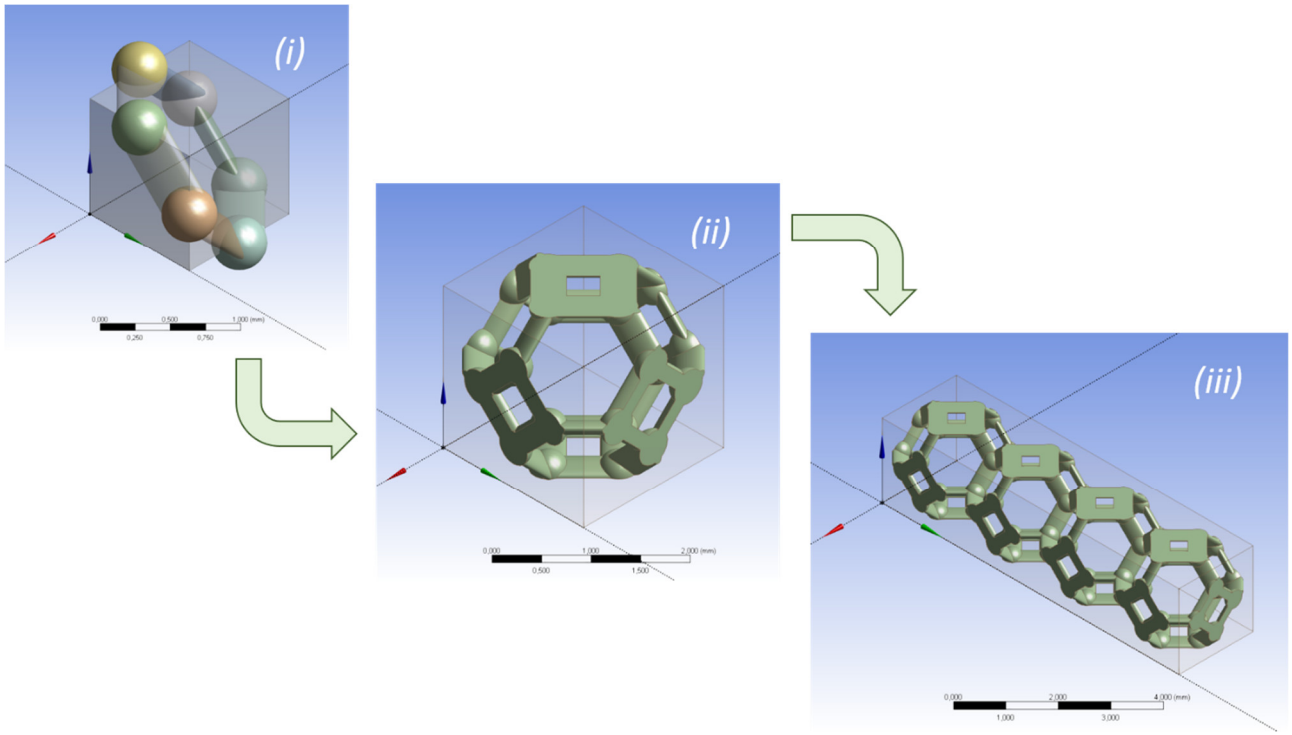

Figure 1. Kelvin cell generation and arrangement process.

Table 1. Kelvin cell elliptical struct foams' design features.

	α	β
E1-1	1.169	0.815
E1-2	1.359	0.556
E2-1	1.227	0.815
E2-2	1.800	0.556

It is clear from Table 1 that the "E2-X" foams presented an α parameter always greater than "E1-X" assuming equal the ratio β.

For the sake of brevity, the other geometrical features were not reported here since they can be retrieved in [27]. Focusing on Figure 1ii, it can be noticed that the bounding cube has a side of 2 mm, corresponding to the diameter of the single cell unit. This implies that the periodical foams have a pore density of 40 PPI, with an almost constant porosity of 0.9 (ranging from 0.88 and 0.9).

The present work also investigated the effects of fiber inclinations (15°, 30°, 45°) (Figure 2) for the four elliptical fiber structures. The configurations with 0° fiber inclination had already been simulated by Moon et al. [27] for all the five fiber structures.

The fiber inclination was defined as the angle (also called "angle of attack", here) between the ellipse's major axis and the main flow direction.

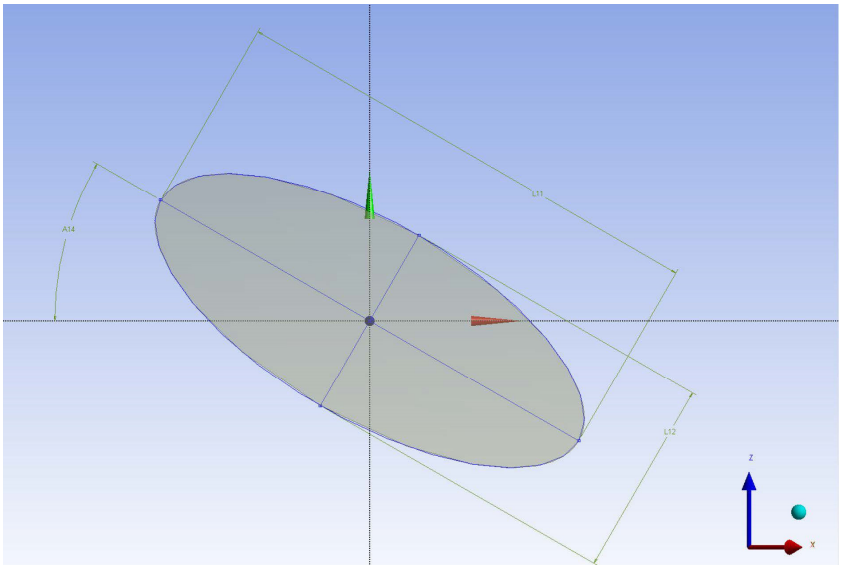

Figure 2. Elliptical fiber inclination angle.

To ensure the fully-developed flow before the air entrance into the foams, an upstream duct of 40 mm was modeled (not at scale in Figure 3, for the sake of visualization). Similarly, a downstream duct with the same length was also added, as shown in Figure 3. Velocities ranging from 0.5 to 4 m s^{-1} and temperature of 298 K were set to the inlet face, resulting in a laminar airflow with Reynolds number based on the strut diameter lower than 300 [27]. The pressure-outlet condition was applied at the exit, setting it at the ambient pressure (gauge pressure of 0 Pa). The up- and downstream ducts were considered adiabatic, therefore no heat or mass exchanges were possible. To heat the system, an aluminum heater of 2×8 mm^2 and thickness of 0.1 mm was modeled; its face was defined as a wall at a constant temperature of 373 K. At both sides of the system, a periodical condition was set. Differently from [27], the present authors modeled half of the entire system. However, since the aim was to replicate the geometry and the operating conditions from [27], the uppermost face was considered as a symmetry plane, and a symmetry boundary condition was adopted consequently. The two systems are perfectly comparable. In Table 2, the material properties as taken from Ansys Fluent 18.2 database are reported.

Table 2. Material main properties.

	Density ($kg\ m^{-3}$)	Specific Heat ($J\ kg^{-1}\ K^{-1}$)	Thermal Conductivity ($W\ m^{-1}\ K^{-1}$)	Viscosity ($kg\ m^{-1}\ s^{-1}$)
Air	ideal-gas	1006.43	0.0261	1.789×10^{-5}
Aluminum	2719	871	237	-

2.2. Numerical Model—Governing Equations

Temperature-dependent properties and a steady state linear ideal gas flow were considered for the numerical model aiming at investigating the heat transfer performance and the hydraulic behavior. For these purposes, the conjugate heat transfer module was used to model the heat transfer between the air and the solid domain (cells' foam and heater). No phase change was taken into account, resulting in a single-phase air flow.

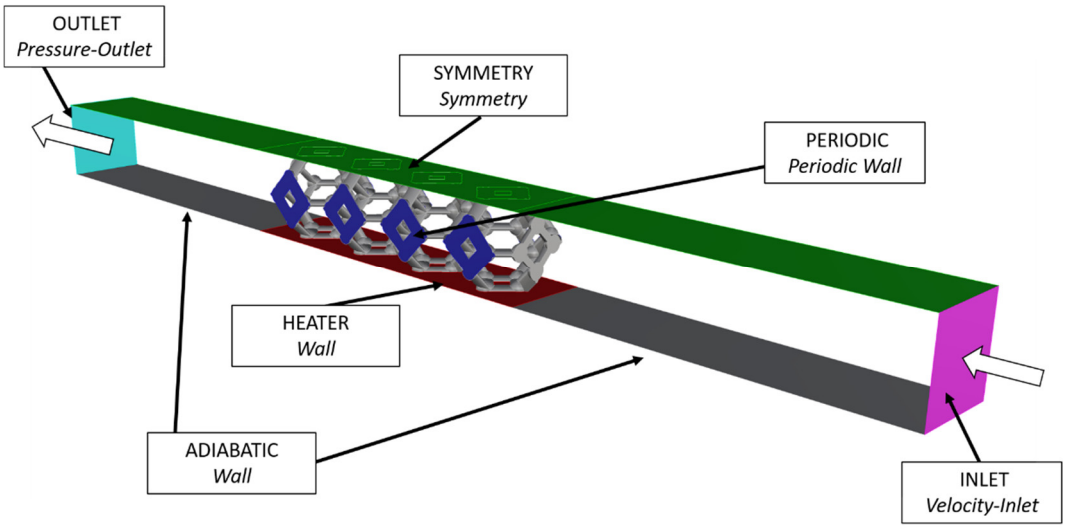

Figure 3. Geometry of the simulated system.

Based on these assumptions, the following three-dimensional conservation equations (Equations (1)–(3)) were solved by means of the CFD software Ansys Fluent 18.2:

$$\nabla \cdot u = 0 \tag{1}$$

$$\rho u \cdot \nabla u = -\nabla p + \mu \cdot \nabla^2 u \tag{2}$$

$$\rho c_p u \cdot \nabla T = k \nabla^2 T \tag{3}$$

where $\boldsymbol{u} = \boldsymbol{u}(x,y,z)$ [(m s^{-1}) is the air velocity vector, ρ (kg m^{-3}) the density, p (Pa) the pressure, μ (Pa·s) the fluid viscosity, c_p (J kg^{-1} K^{-1}) the specific heat, k (W m^{-1} K^{-1}) the thermal conductivity, T (K) the fluid temperature.

2.3. Numerical Model—Mesh Sensitivity Analysis and Model Validation

In order to demonstrate the model reliability and solution independence from the grid, a mesh sensitivity analysis was conducted. Among the five configurations investigated by Moon et al. [27], the present authors decided to validate the developed numerical model on the results for the E1-2 configuration with 0° fiber inclination angle and cylindrical shape. For what concerns the solution independence from the grid, the E1-2 was adopted as reference case. The comparison was made in terms of friction factor f and thermal power Q for all the five velocities analyzed, as defined below [27]:

$$f = \frac{\Delta P}{L} \frac{D}{2\rho_f U_{in}^2} \tag{4}$$

$$Q = \dot{m} c_{p,f} (T_{out} - T_{in}) \tag{5}$$

where $\frac{\Delta P}{L}$ is the pressure gradient (Pa m^{-1}), D the hydraulic diameter (m), and $\dot{m}$ the mass flow rate (kg s^{-1}). The subscript f refers to the fluid, i.e., air.

Three different meshes were simulated. The coarsest one, denoted as "Mesh 1" in Figure 4, consisted of some 6.2 M elements. "Mesh 2" 10.4 M and "Mesh 3" 18.3 M elements, respectively. As it can be observed from Figure 4, the coarsest mesh resulted in friction factor and thermal power values that deviated from Moon et al. [27] results by more than −10% (see the lower dotted line). Mesh 2 and Mesh 3, instead, showed f and Q values that differed less than 10% with respect to [27]. From what was calculated, the present authors decided to consider Mesh 2 as the best trade-off between solution accuracy and computational efforts. Therefore, the other meshes for all the other cases were obtained by

adopting the same characteristics of Mesh 2. In Table 3, the number of elements for all the cases is reported.

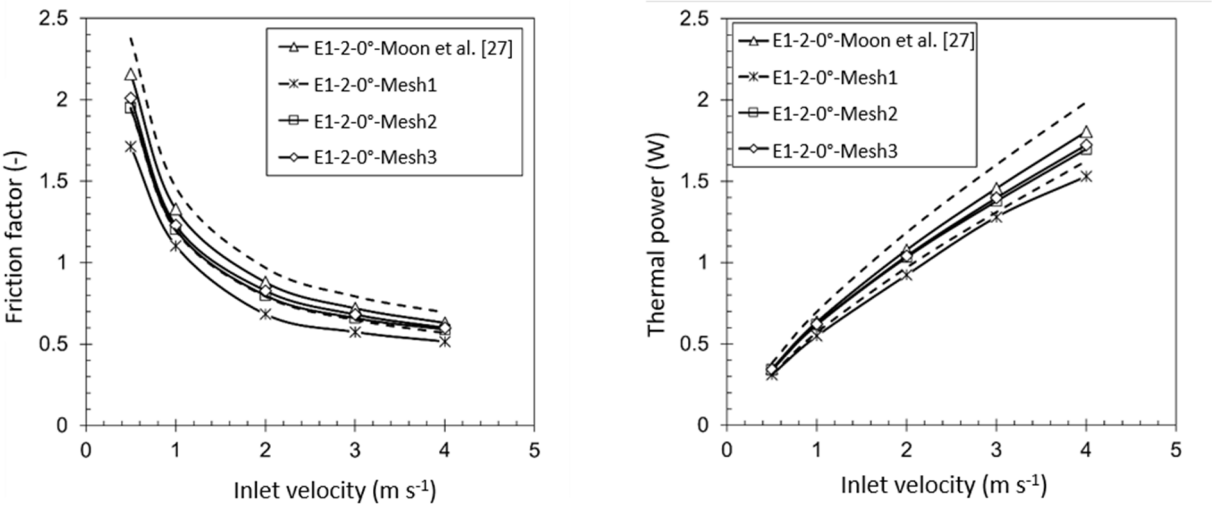

(**a**) (**b**)

Figure 4. Mesh sensitivity analysis: (**a**) Friction factor and (**b**) thermal power.

Table 3. Mesh number elements ($\bullet 10^6$) for all the simulated cases.

	0°	15°	30°	45°
C_0	6.4	-	-	-
E1-1	5.5	5.5	5.7	5.7
E1-2	10.4	10.6	10.3	10.1
E2-1	6.1	6.2	6.2	6.2
E2-2	10.5	11.5	11.0	13.9

Figure 5 clearly demonstrates the validity of the developed numerical model. As shown in Figure 5a, the friction factor deviates less than 10% (represented by the dotted lines) from Moon et al.'s [27] results, both for the elliptical and cylindrical configurations. Moreover, the results for the cylindrical case differ less than 3.5% with respect to the results for the same case [27]. Even for the thermal power Q, similar conclusion can be taken. Our simulated cases deviate no more than 4% from what reported in [27] for all the investigated scenarios. The minor differences between the results may be attributed to a different numerical model generation: in fact, as explained above, differently from Moon et al. [27], the present authors studied half of the geometrical domain, taking advantage of the symmetry of the system. Therefore, despite the small deviations, the present numerical model can be considered a valid alternative requiring almost half of the computational effort which can have a positive effect on computational efficiency allowing for the possibility of investigating many additional cases.

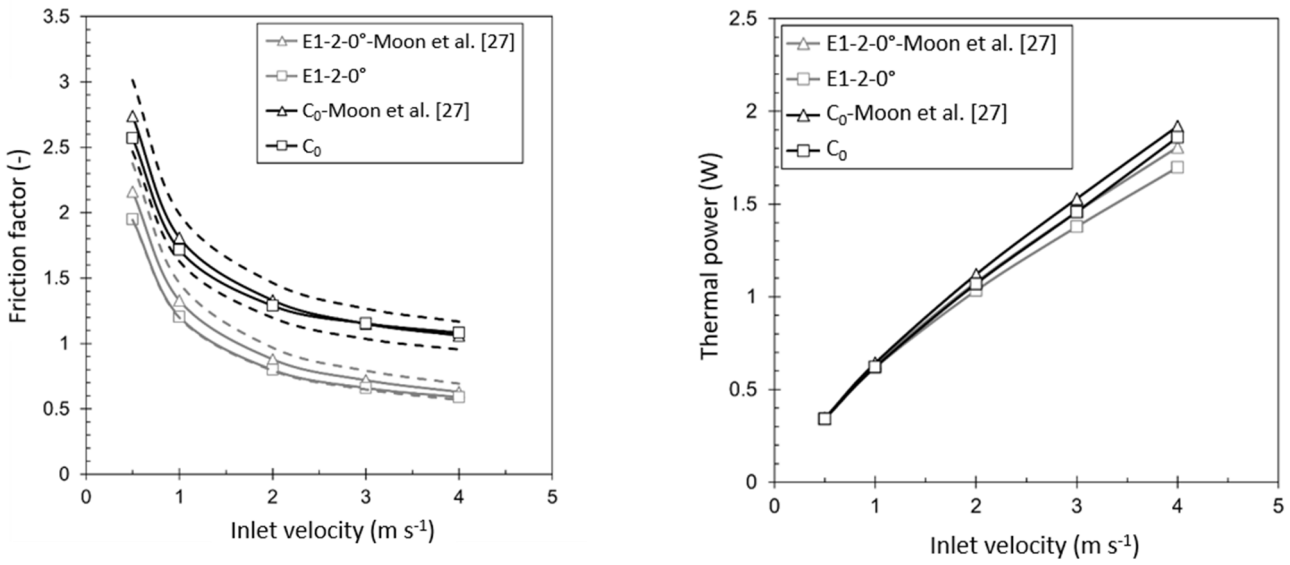

(**a**) (**b**)

Figure 5. Model validation: (**a**) Friction factor and (**b**) Thermal power.

3. Results

As shown in Figure 6a,b, an additional plane (denoted as "Plane+") was used to capture the velocity, pressure and temperature contours inside the foams. The plane was inclined of 45° with respect to the horizontal axis in order to comprehensively investigate the hydraulic and thermal performances of the air crossing the periodic aluminum foams.

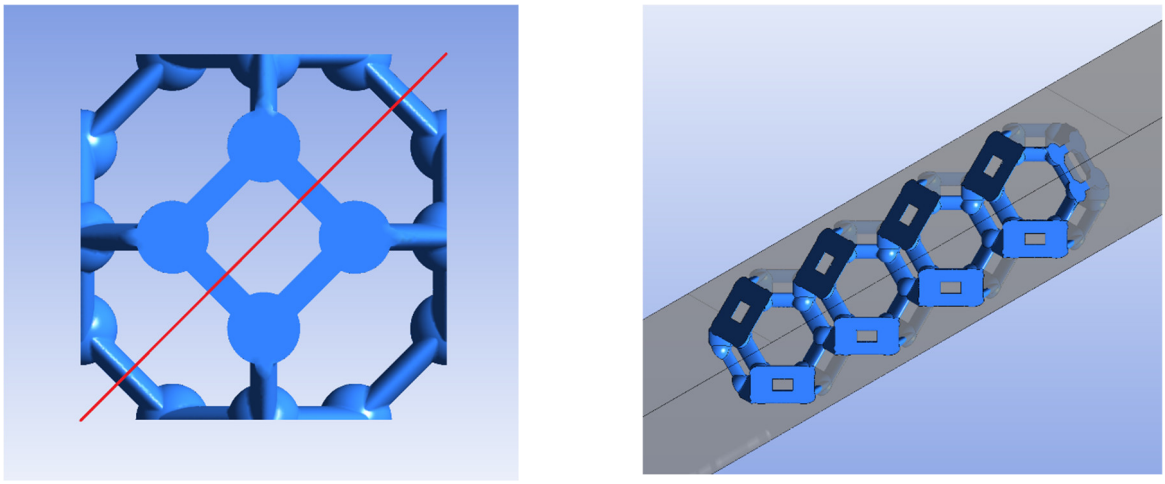

(a) (b)

Figure 6. Plane+ (**a**) 2D and (**b**) 3D sections.

To analyze the effect of the elliptical fiber orientation on the heat transfer and pressure drops with respect to the reference circular strut (subscript "0"), the ratios of Colbourn numbers $\frac{j}{j_0}$ and friction factors $\frac{f}{f_0}$ as function of the air mass velocity (G) were used, respectively. The friction factor f was calculated by Equation (4), while the Colbourn number j was obtained by means of the following equation:

$$j = \frac{HTC}{\rho_f c_{p,f} u} \left(\frac{c_{p,f} \mu_f}{k_f} \right)^{\frac{2}{3}} \quad (6)$$

HTC (W m^{-2} K^{-1}) is the interstitial convective heat transfer coefficient defined as the ratio between the thermal power Q (see Equation (5)) and the total heat transfer area A multiplied by the logarithmic mean temperature difference ΔT_{log}, as shown in Equation (7):

$$HTC = \frac{Q}{\Delta T_{log} A} \tag{7}$$

$$\Delta T_{log} = \frac{T_{out} - T_{in}}{\ln \frac{T_h - T_{in}}{T_h - T_{out}}} \tag{8}$$

G (kg m^{-2} s^{-1}), mass velocity, is defined as the product between the air density and the air velocity:

$$G = \rho_f u \tag{9}$$

As shown in Figure 7, results for E2-1, E1-2, and E2-2 were reported. To avoid redundancy, graphs for E1-1 foams were not considered due to their strong geometrical similarity and thermal-hydraulic behavior with E2-1 ones (see Table 1).

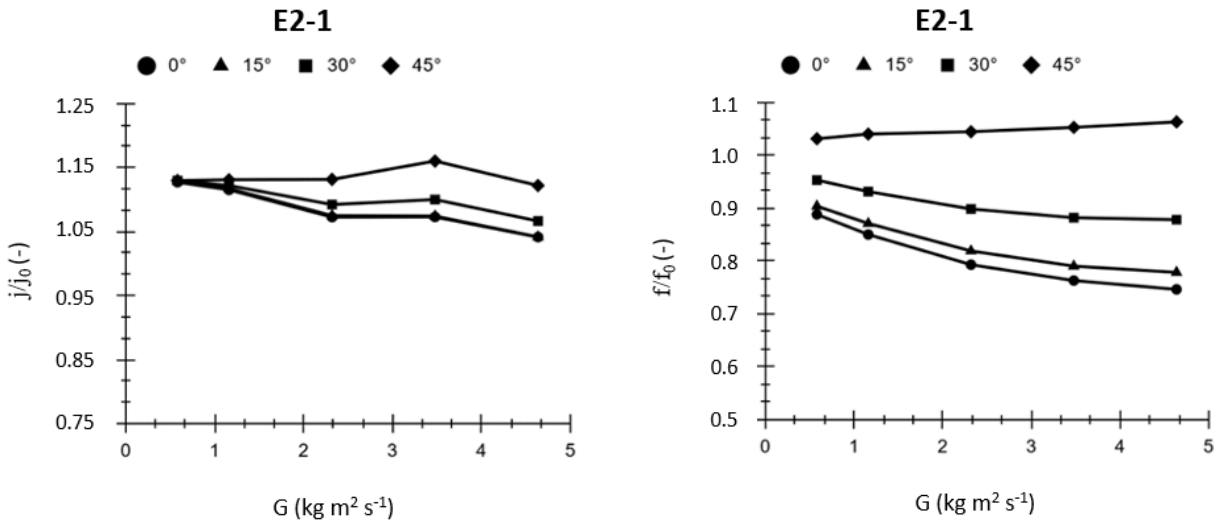

(**a**) (**b**)

Figure 7. *Cont.*

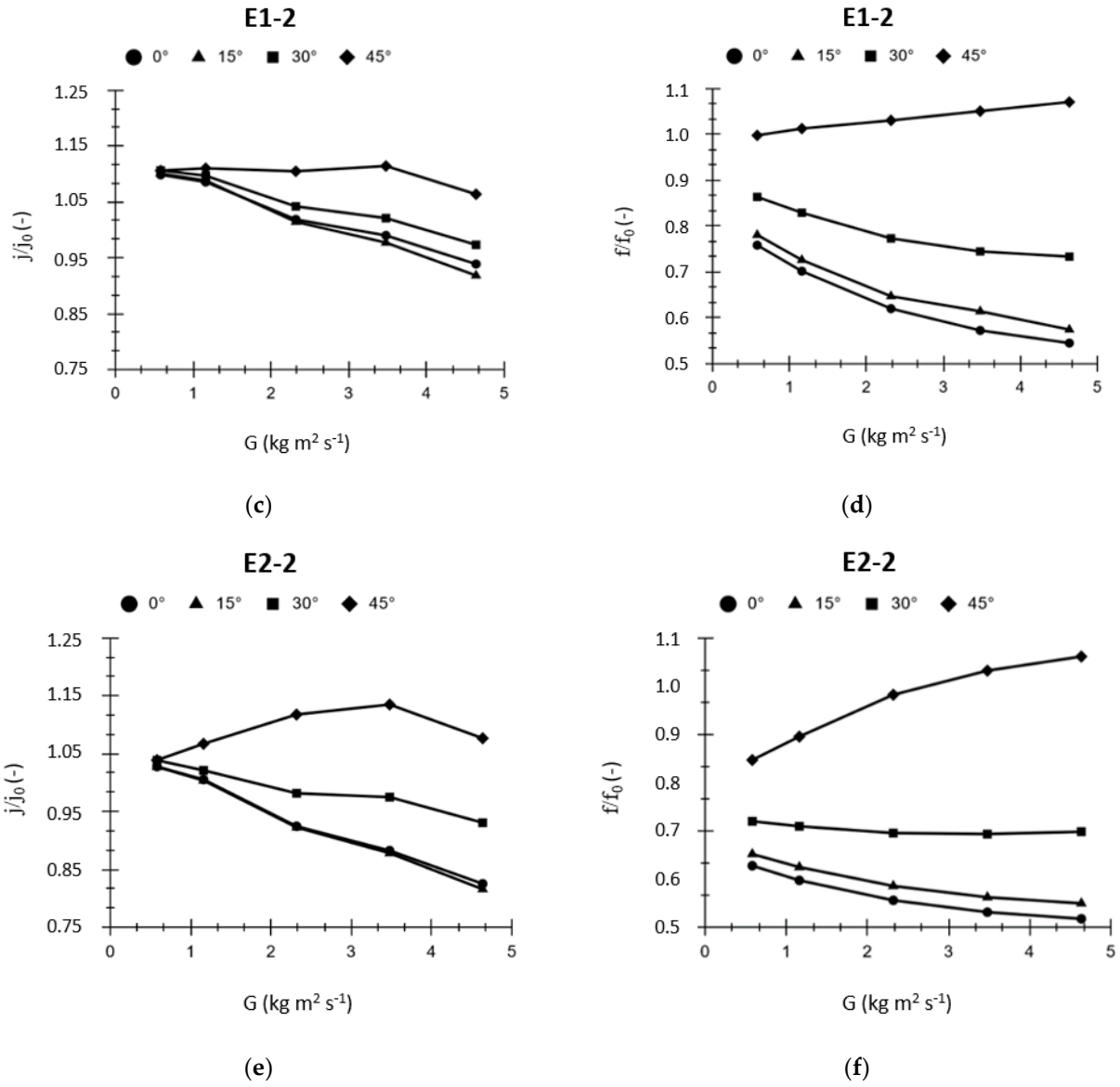

Figure 7. Colbourn numbers ratio for (**a**) E2-1, (**c**) E1-2, (**e**) E2-2. Friction factors ratio for (**b**) E2-1, (**d**) E1-2, (**f**) E2-2.

Focusing on the heat transfer performance, it is interesting to notice that the elliptical E2-1 foams (Figure 7a) outperformed the reference circular ones for all the investigated angles of attack at all the air mass velocities. In fact, the ratio j/j_0 is always greater than 1. However, it must be underlined that while 0–15–30° show a substantial decrease of the rate of heat transfer enhancement as the velocity increases, the 45° cases show a growing enhancement rate only up to 3 m s^{-1} and then they start decreasing with a slope comparable with other fibers' inclination. Hence, inlet velocity equals to 3 m s^{-1} can be considered as the point of maximum. The same trends were obtained for E1-2 (Figure 7c) and E2-2 (Figure 7e).

This phenomenon can be explained by investigating the contours of air velocity inside the foams before the 3 m s^{-1} (i.e., 2 m s^{-1} inlet velocity) (Figure 8a,c,e,g) and this value (i.e., 4 m s^{-1} inlet velocity) (Figure 8b,d,f,h). At 2 m s^{-1}, the highest value of the velocity through the fibers grows as the orientation increases. In fact, it can be noticed that from 0° (Figure 8a) to 45° (Figure 8g), the maximum velocity increases from 5.15 m s^{-1} to 6.17 m s^{-1}. Therefore, the increasing tortuosity could justify the enhancement of the heat transfer due to the continuous mixing of the fluid. Nevertheless, considering 4 m s^{-1} inlet velocity something different can be inferred. All the foams show longer stagnation zones behind

the fibers, i.e., dead zone. The stagnation zones can be detrimental for the heat transfer, because extremely low velocities cause the convective heat transfer coefficient to decrease. Moreover, for 4 m s^{-1}, the local maximum velocity is not completely developed as it was for 2 m s^{-1}. The worst case is reached with 45° fibers' inclination (Figure 8h) because the velocity achieves its maximum value only in the central zones of the periodic foam.

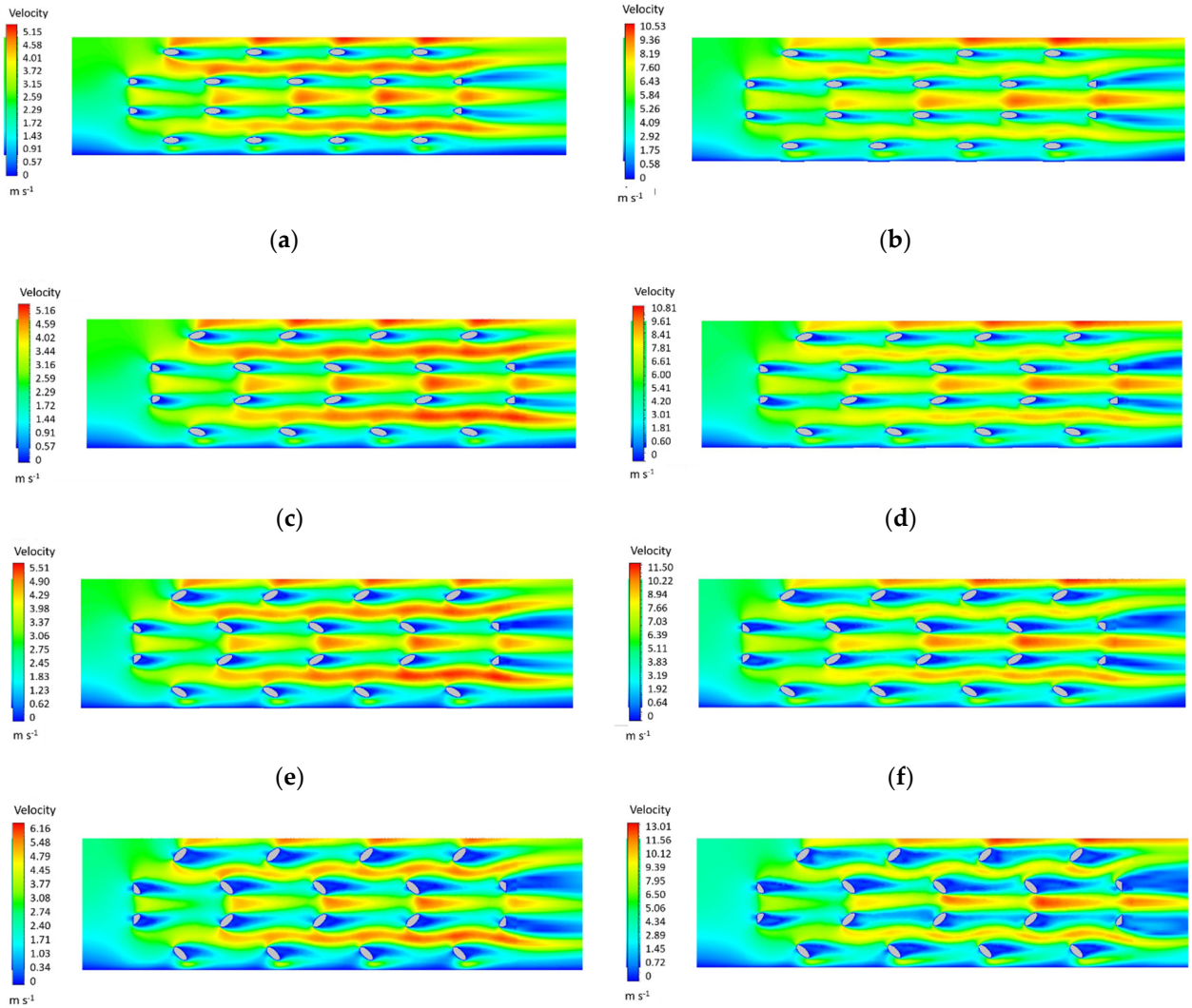

Figure 8. Velocity contours for E1-2 at 2 m s^{-1} (**a**,**c**,**e**,**g**) and 4 m s^{-1} (**b**,**d**,**f**,**h**).

In Figure 9, the negative effect of the stagnation zones can be appreciated. In fact, as shown in Figure 9a, the air temperature behind the fibers is higher if compared with air temperature shown in Figure 9b. Despite that, the latter presents a j/j_0 ratio which is over the unity (1.064). This means that E1-2, 45° performs better than the reference circular struts even at the highest investigated velocity.

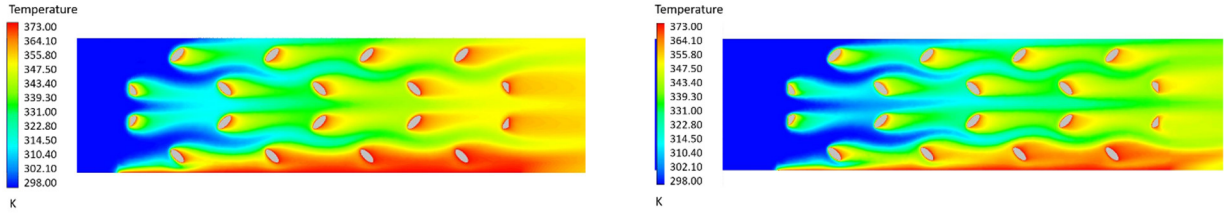

(**a**) (**b**)

Figure 9. Temperature contours for E1-2, 45°, at 2 m s^{-1} (**a**) and 4 m s^{-1} (**b**).

Nevertheless, when considering a possible application of heat exchangers adopting periodic open cell metal foams, it is needed to deeply investigate even the hydraulic performance of periodic foams.

From Figure 7b,d,f, it can be noticed that the elliptical foams, up to 30° fiber inclination, present lower (or, at most, equal) friction factors if compared with the reference structures. Moreover, the friction factor ratios tend to decrease as the velocity increases. Only the 45° oriented struts show f/f_0 always greater than 1 for all the 5 investigated inlet velocities. When comparing the velocity contours at fixed inlet velocity (for example, 4 m s^{-1}, Figure 8b,d,f,h, it is clear that, as the angle attack increases, a greater frontal fiber surface is seen by the airflow. Therefore, the greater frontal surface acts as an additional obstacle to the main flow. If the inclination of 45° (Figure 8h) is likened to 0° (Figure 8b), it is evident how the stagnant zones are remarkably more extended in the first case as compared to the second one, justifying the increase in pressure drops (in terms of friction factors). From the hydraulic performance point of view, the elliptical E2-2 Kelvin cell-based metal foam (Figure 7f) can be considered the worst case: in fact, 30° presents a f/f_0 curve which flattens along the unity, meaning that no hydraulic performance improvement can be obtained with respect to the circular struts' reference foam. Moreover, even worse, 45° (Figure 7f) shows a noticeable increase in f/f_0 curve which, at 4 m s^{-1}, is almost two times higher than the value for reference case (f/f_0 = 1.904).

For the same orientation and inlet velocity values, E1-2 has only some of 7% greater friction factor value as compared to C0 (f/f_0 = 1.071).

The relevant different hydraulic behavior can be attributed to their intrinsic geometrical properties. From Table 1, it can be noticed that both foams present the same β (0.556) but different α (1.359 for E1-2, 1.800 for E2-2). A greater α results in a higher frontal surface seen by the air, causing additional flow disturbances and flow restrictions (Figure 10) as well as an increase in abrupt pressure drops (Figure 11), consequently. Besides, more inhomogeneous pressure gradients can be observed for E2-2 if compared with E1-2, thus affecting the hydraulic behavior negatively.

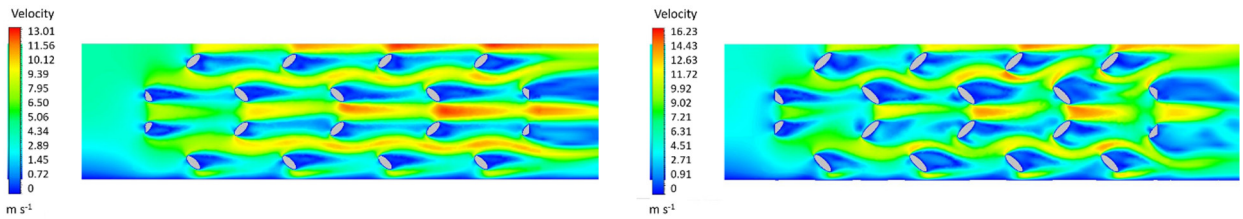

(**a**) (**b**)

Figure 10. Velocity contours for (**a**) E1-2 and (**b**) E2-2, 45° 4 m s^{-1}.

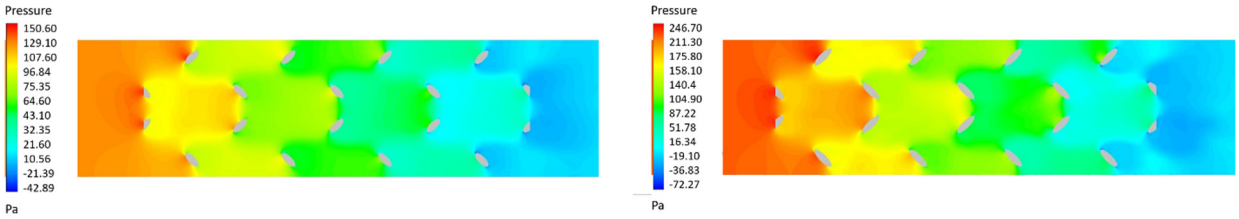

(**a**) (**b**)

Figure 11. Pressure contours for (**a**) E1-2 and (**b**) E2-2, 45° 4 m s^{-1}.

As shown in Figure 11b, E2-2 can have local pressure gradients which can be some of 65% higher than E2-1. In fact, a maximum local pressure difference of 246.7 Pa was calculated for E2-2, being 150.6 Pa for E1-2.

By employing the Darcy–Forcheimer equation (Equation (10)), which approximates the pressure gradient's curve with a second-order function of the parameter χ defined as the product of the foam porosity and the inlet velocity, the permeability K (Equation (11)) and the Forcheimer coefficient φ (Equation (12)) for all the simulated geometries can be calculated, and the results are reported in Figure 12.

$$\frac{\Delta P}{L} = c_1\chi + c_2\chi^2 \tag{10}$$

$$K = \frac{\mu_f}{c_1} \tag{11}$$

$$\varphi = \frac{c_2}{\rho_f} \tag{12}$$

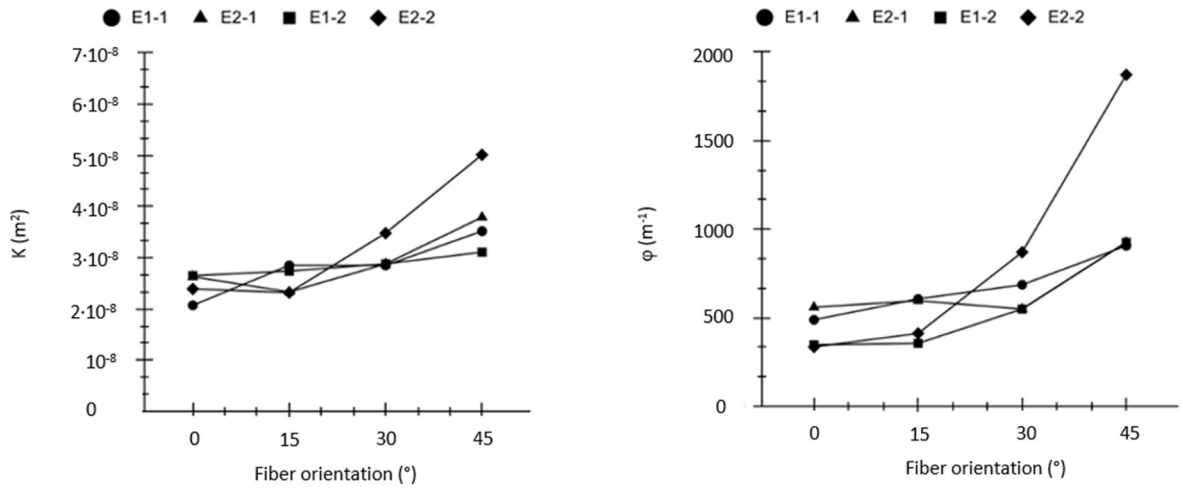

(**a**) (**b**)

Figure 12. K (**a**) and φ (**b**) trends as function of the fiber orientation.

For the sake of brevity, only the values of pressure gradients for E1-2 and E2-2 were reported in Figure 13.

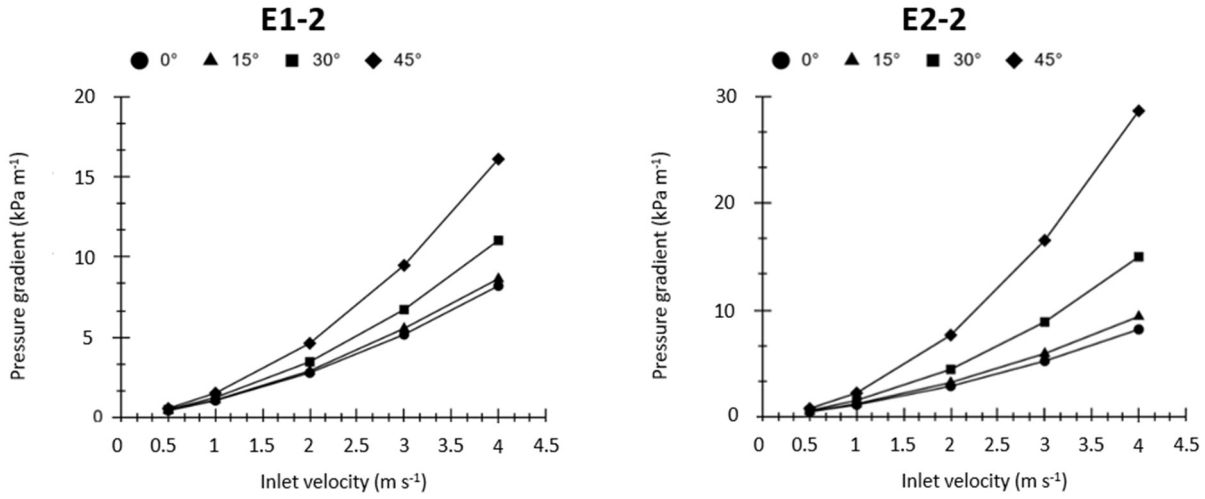

(**a**) (**b**)

Figure 13. Pressure drop trends as function of inlet velocity for (**a**) E1-2 and (**b**) E2-2.

It can be appreciated that for all the fiber orientations, the pressure drops have a parabolic trend, which is in line with Equation (10). As the angle of attack increases, for a given inlet velocity, the pressure gradient increases. In fact, as shown in Figure 12, 45° fiber inclination foams present greater values of K and φ if compared against the same geometry at lower angles of attack. It can be concluded that, from a hydraulic point of view, an increase of the angle of attack results in a pressure drop increase.

Nevertheless, aiming at establishing the best thermal performance among the different investigated configurations, it is interesting to analyze the interstitial HTC (Equation (7)) as a function of the pumping power per area density (PPD) (W m^{-2}). This parameter is defined as the ratio between the product of pressure drops ΔP (Pa) and volumetric flow rate $\dot{V}$ (m^3 s^{-1}), and heat transfer area A (m^2) as given by:

$$PPD = \frac{\Delta P \, \dot{V}}{A} \tag{13}$$

From Figure 14, the results show that E1-1 and E1-2 (which are very similar, see Table 1) present a better thermal performance if compared with other configurations. Assuming a constant value for the PPD, E1-1 and E1-2 give a value for HTC which is always higher, for all the investigated fiber orientations.

Nevertheless, considering a possible implementation of periodic cell metal foams in real applications, it is fundamental to analyze the global performance of the foams. In particular, it must be taken into account the contemporary needs of high thermal transfer characteristics and low pressure drops. Usually, a trade-off between these two conflicting needs must be found.

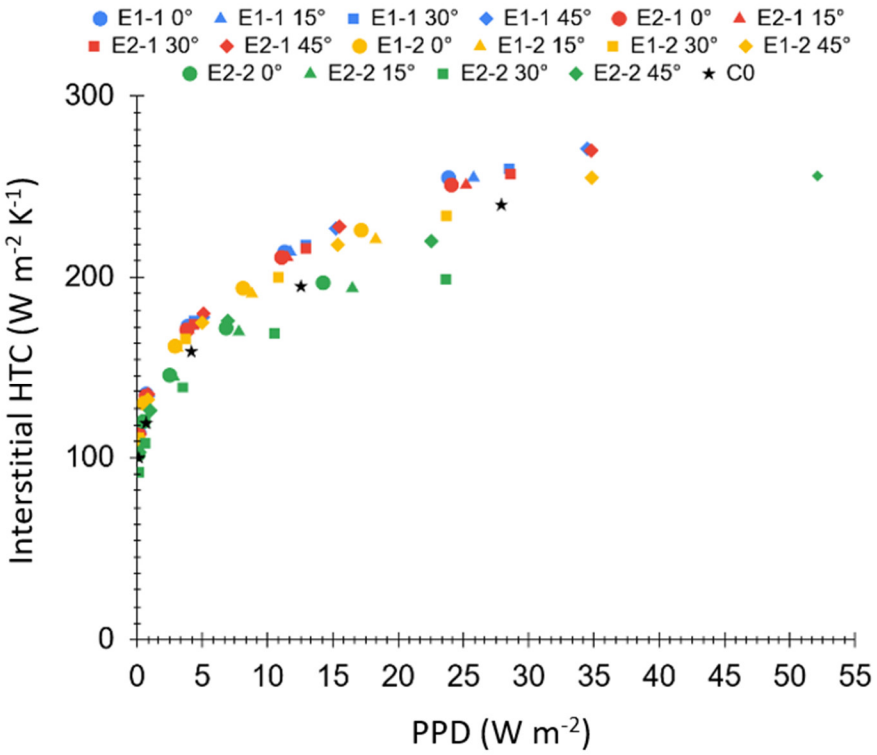

Figure 14. HTC as function of PPD curves' trend for all the investigated KMFs' configurations.

Therefore, among the possible Performance Evaluation Criteria (PEC) [28], the following one, as reported in Equation (14), was used as a function of Reynolds number (Equation (15)), to compare the different configurations:

$$PEC = \frac{\frac{j}{j_0}}{\left(\frac{f}{f_0}\right)^{\frac{1}{3}}} \quad (14)$$

$$Re = \frac{\rho D u}{\mu \varepsilon} \quad (15)$$

$$D = \frac{4l^2}{3l} \quad (16)$$

Focusing on Figure 15, the PEC as function of Re can be appreciated. It is evident that the elliptical struts overcome the circular ones for almost all the investigated configurations. Only E2-2 30° and 45° present PEC values lower than C0. For all the Kelvin cell- based metal foams, the global performance becomes worse as the fiber inclination increases for all the Re numbers. As already explained, higher angles of attack led to a better thermal performance at the expanse of pressure drop. Therefore, if interested in evaluating the global enhancement of the thermal-hydraulic behavior of the elliptical struts' foams with respect to circular ones, E1-2 with 0° angle of attack can be proposed as the best compromise, reaching a PEC value which is 22% higher than that for reference case, at Re = 200.

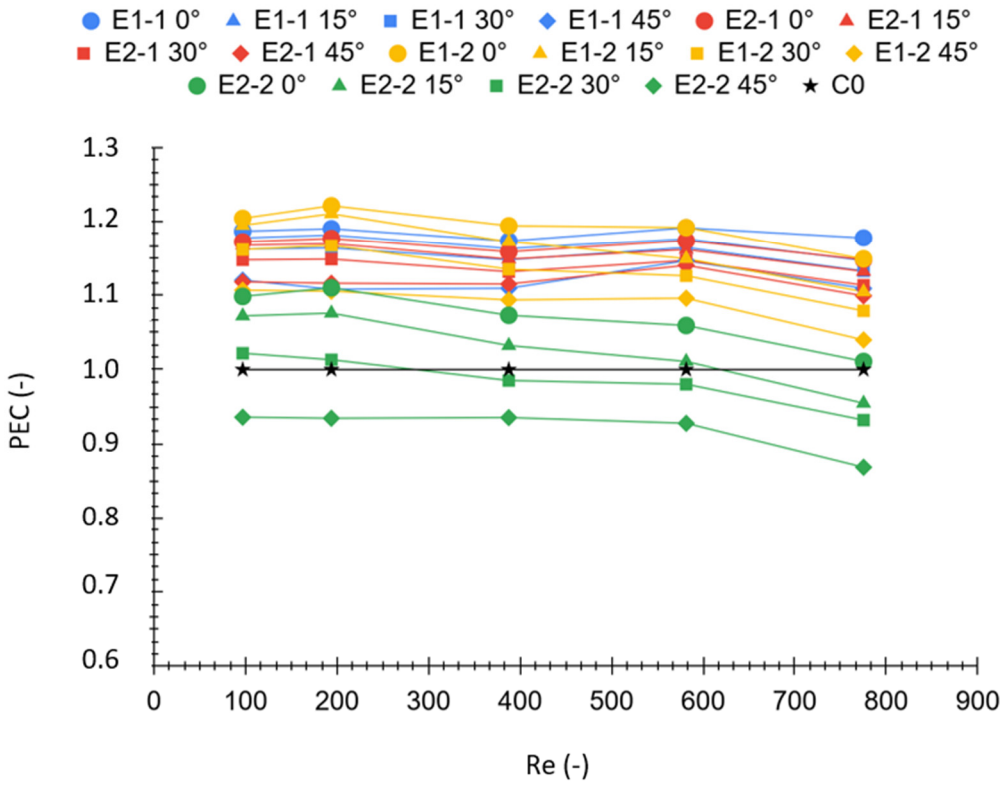

Figure 15. PEC as function of Re for all the investigated KFMs' configurations.

4. Conclusions

In this work, the possibility of increasing heat transfer in periodic Kelvin cell-based aluminum foams by considering fiber inclination effect was investigated. Four angles of attack (fibers' orientation with respect to main air flow) were analyzed: 0°, 15°, 30°, 45° for four elliptical struts' (E1-1, E2-1, E1-2, E2-2) configurations. In particular, by means of steady state numerical simulations in Ansys Fluent environment, the thermal-hydraulic behavior was studied and deeply discussed by varying the air inlet velocities (0.5, 1, 2, 3, 4 m s^{-1}). Besides, the results were compared in terms of enhanced performances with respect to the circular struts' foams considered as reference case.

A PEC was used to directly compare the foam configurations. Results revealed that, as the angle of attack increased, a general reduction of the overall performance enhancement was obtained due to a remarkable flow disturbance if compared to no inclination cases. It can be concluded that almost all elliptical struts investigated performed better than circular ones (except E2-2 30° and 45°). More specifically, the best result was obtained for E1-2 with 0° angle of attack, which reached a PEC value which is 22% higher than that for reference case, at Re = 200.

Author Contributions: M.C.: Conceptualization, methodology, investigation, software, writing—original draft preparation. E.D.M.: Investigation, software, writing—review and editing. S.M.: Conceptualization, supervision, methodology, writing—review and editing. All authors have read and agreed to the published version of the manuscript.

Funding: This research received no external funding.

Acknowledgments: The authors wish to acknowledge the support and the computational resources made available by the High Performance Computing Lab at the Department of Management and Engineering (DTG), co-funded by the University of Padova in the framework of the program "Scientific Research Instrumentation 2015".

Conflicts of Interest: The authors declare no conflict of interest.

References

1. Mancin, S.; Zilio, C.; Cavallini, A.; Rossetto, L. Pressure drop during air flow in aluminium foams. *Int. J. Heat Mass Transf.* **2010**, *53*, 3121–3130. [CrossRef]
2. Mancin, S.; Zilio, C.; Rossetto, L.; Cavallini, A. Heat transfer performance of aluminium foams. *J. Heat Transf.* **2011**, *133*, 060904. [CrossRef]
3. Mancin, S.; Zilio, C.; Cavallini, A.; Rossetto, L. Heat transfer during air flow in aluminium foams. *Int. J. Heat Mass Transf.* **2010**, *53*, 4976–4984. [CrossRef]
4. Lu, W.; Zhao, C.; Tassou, S. Thermal analysis on metal-foam filled heat exchangers, Part I: Metal foam filled pipes. *Int. J. Heat Mass Transf.* **2006**, *49*, 2751–2761. [CrossRef]
5. Incera Garrido, G.; Patcas, F.C.; Lang, S.; Kraushaar-Czarnetzki, B. Mass transfer and pressure drop in ceramic foams: A description for different pore sizes and porosities. *Chem. Eng. Sci.* **2008**, *63*, 5202–5217. [CrossRef]
6. Yu, N.; Tee, C.C.; Li, H. Thermal properties of graphite foam: Experiments and modelling. In Proceedings of the 7th Biennal Conference on Engineering Systems Design and Analysis, Manchester UK, 19–22 July 2004; Volume 1, pp. 383–386.
7. Kim, S.Y.; Kang, B.H.; Kim, J.-H. Forced convection from aluminium foam materials in an asymmetrically heated channel. *Int. J. Heat Mass Transf.* **2001**, *44*, 1451–1454. [CrossRef]
8. Zhao, C.Y.; Kim, T.; Lu, T.J.; Hodson, H.P. Thermal properties in high porosity metal foams. *J. Thermophys. Heat Transf.* **2004**, *18*, 309–317. [CrossRef]
9. Abadi, G.B.; Moon, C.; Kim, K.C. Experimental study on single-phase heat transfer and pressure drop of refrigerants in a plate heat exchanger with metal-foam filled channels. *Appl. Therm. Eng.* **2016**, *102*, 423–431. [CrossRef]
10. Kumar, P.; Topin, F. Micro-structural impact of different strut shapes and porosity on hydraulic properties of Kelvin-like metal foams. *Trans. Porous Media* **2014**, *105*, 57–81. [CrossRef]
11. Yang, L.; Harrysson, O.; Cormier, D.; West, H.; Gong, H.; Stucker, B. Additive manufacturing of metal cellular structures: Design and fabrication. *Jom* **2015**, *67*, 608–615. [CrossRef]
12. Thompson, M.K.; Moroni, G.; Vaneker, T.; Fadel, G.; Cambpell, R.I.; Gibson, I.; Bernard, A.; Schulz, J.; Graf, P.; Ahuja, B. Design for Additive manufacturing: Trends, opportunities, considerations, and constraints. *CIRP Ann.* **2016**, *65*, 737–760. [CrossRef]
13. Righetti, G.; Savio, G.; Meneghello, R.; Doretti, L.; Mancin, S. Experimental study of phase change material (PCM) embedded in 3D periodic structure realized via additive manufacturing. *Int. J. Therm. Sci.* **2020**, *153*, 106376. [CrossRef]
14. Piili, H.; Happonen, A.; Vaisto, T.; Venkataramanan, V.; Partanen, J.; Salminen, A. Cost estimation of laser additive manufacturing of stainless stell. *Phys. Procedia* **2015**, *78*, 388–396. [CrossRef]
15. Lord Kelvin. On the division of space with minimum partitional area. *Acta Math.* **1887**, *11*, 121–134. [CrossRef]
16. Weaire, D.; Phelan, R. A counter-example to Kelvin's conjecture on minimal surfaces. *Philos. Mag. Lett.* **1994**, *69*, 107–110. [CrossRef]
17. Du Plessis, J.P.; Masliyah, J.H. Mathematical modelling of flow through consolidated isotropic porous media. *Transport Porous Med.* **1994**, *49*, 3545–3553. [CrossRef]
18. Lu, T.J.; Stone, H.A.; Ashby, M.F. Heat transfer in open-cell metal foams. *Acta Mater.* **1998**, *46*, 3619–3635. [CrossRef]
19. Huu, T.T.; Lacroix, M.; Huu, C.P.; Schweich, D.; Edouard, D. Towards a more realistic modelling of solid foam: Use of pentagonal dodecahedron geometry. *Chem. Eng. Sci.* **2009**, *64*, 5131–5142. [CrossRef]
20. Bai, M.; Chung, J.N. Analytical and numerical prediction of heat transfer and pressure drop in open-cell metal foams. *Int. J. Therm. Sci.* **2011**, *50*, 869–880. [CrossRef]
21. Wu, Z.; Caliot, C.; Bai, F.; Flamant, G.; Wang, Z.; Zhang, J.; Tian, C. Experimental and numerical studies of the pressure drop in ceramic foams for volumetric solar receiver applications. *Appl. Energy* **2010**, *87*, 504–513. [CrossRef]
22. Cunsolo, S.; Iasiello, M.; Oliviero, M.; Bianco, N.; Chiu, W.K.S.; Naso, V. Lord Kelvin and Weaire-Phelan foam models: Heat transfer and pressure drop. *J. Heat Transf.* **2016**, *138*, 022601. [CrossRef]
23. Mancin, S.; Zilio, C.; Diani, A.; Rossetto, L. Experimental air heat transfer and pressure drop through copper foams. *Exp. Therm. Fluid Sci.* **2012**, *36*, 224–232. [CrossRef]
24. Mancin, S.; Zilio, C.; Diani, A.; Rossetto, L. Air forced convection through metal foams: Experimental results and modelling. *Int. J. Heat Mass Transf.* **2013**, *62*, 112–123. [CrossRef]
25. Iasiello, M.; Cunsolo, S.; Oliviero, M.; Harris, W.M.; Bianco, N.; Chiu, W.K.; Naso, V. Numerical analysis of heat transfer and pressure drop in metal foams for different morphological model. *J. Heat Transf.* **2014**, *136*, 112601. [CrossRef]
26. Ambrosio, G.; Bianco, N.; Chiu, W.K.S.; Iasiello, M.; Naso, V.; Oliviero, M. The effect of open-cell metal foams strut shape on convection heat transfer and pressure drop. *Appl. Therm. Eng.* **2016**, *103*, 333–343. [CrossRef]
27. Moon, C.; Kim, H.D.; Kim, K.C. Kelvin-cell-based metal foam heat exchanger with elliptical struts for low energy consumption. *Appl. Therm. Eng.* **2018**, *144*, 540–550. [CrossRef]
28. Webb, R.L. *Principles of Enhanced Transfer*; Taylor and Francis: New York, NY, USA, 2005.